Available online at www.sciencedirect.com

ScienceDirect

Procedia Manufacturing 34 (2019) 867–875

Procedia MANUFACTURING

www.elsevier.com/locate/procedia

47th SME North American Manufacturing Research Conference, Penn State Behrend Erie, Pennsylvania, 2019

Displacement-based dynamometer for milling force measurement

Michael F. Gomez and Tony L. Schmitz*

University of North Carolina at Charlotte, Mechanical Engineering and Engineering Science, Charlotte, NC, 28223, USA

* Corresponding author. Tel.: +-704-687-5086; fax: +704-687-8345. *E-mail address:* tony.schmitz@uncc.edu

Abstract

This paper presents a novel method for measuring cutting forces during milling using a flexure-based dynamometer. The flexure displacement is measured and the force is determined by structural deconvolution. In this approach, the force is extracted from displacement by filtering the displacement signal in the frequency domain using the flexure's displacement-to-force frequency response function. It is shown that, for a range of excitation forces, the measured displacement can be used to reconstruct the force profile. First, a single degree of freedom flexure system is used to determine the excitation forces. Second, the structural deconvolution technique is applied to a multiple degree of freedom flexure system. Finally, a cutting force comparison is made between a multi-axis piezoelectric dynamometer and the reconstructed displacement-based force profile. Good agreement between measured and reconstructed forces is demonstrated.

Keywords: Machining; force; frequency response function; dynamometer

1. Introduction

Cutting force measurement and modeling is fundamental to improved understanding of machining processes. In practice, multi-axis dynamometers based on piezoelectric sensors provide the most common solution for cutting force measurement [1-2]. The dynamic deflections of the dynamometer's piezo-electric load cells during machining operations produce a charge proportional to their deformation [3]. However, the dynamic properties of the dynamometer must be considered when operating at or near the dynamometer's natural frequencies. At the natural frequencies there is an artificial amplification of force signals which can lead to inaccurate force readings. The measured cutting force can be compensated by filtering using the dynamometer force-to-input force transmissibility [1, 3-5]. In doing so, there is a structural deconvolution of the unwanted dynamometer dynamics from the measured force signals. As a result, the structural dynamics of the system determine the achievable measurement bandwidth [1].

Given these measurement limitations, research efforts have addressed alternative force measuring dynamometer designs. Schmitz *et al.* [6] presented a high frequency (10 kHz-16 kHz) dynamometer based on two coupled, single degree-of-freedom (SDOF) flexures which interact to produce vibration modes at the bandwidth of interest. Yaldiz *et al.* [7] described the development of a four-component dynamometer to measure static and dynamic cutting forces and torque using strain-gauge based sensors. Transchel *et al.* [8] developed a high frequency (up to 5 kHz) dynamometer where sensitive piezoelectric sensors were pre-loaded with a common bolt resulting an improved dynamic stiffness. Totis *et al.* [9] developed a plate-type dynamometer using three high-sensitivity tri-axial piezoelectric force sensors. The novel sensor configuration provided higher natural frequencies and, therefore, increased bandwidth. Ettrichratz *et al.* [10] presented a novel cutting force measurement using piezoceramic layers applied on a carbide sensor plate that was mounted next to a cutting insert. In doing so, the force measurement was moved closer to the cutting point of contact.

10.1016/j.promfg.2019.06.161

Alternative approaches for accurate cutting force measurement include post-processing of measured force data to remove the structural dynamics of the dynamometer. Altintas and Park [11] designed a Kalman filter to remove the structural dynamic influence of the spindle transfer functions. In this case, piezoelectric force sensors were integrated into a spindle housing to measure and identify cutting forces. Castro *et al.* [3] attenuated high frequency amplification due to "cross-talk" between the dynamometer's component axes through the system's transmissibility matrix. Ozdoganlar *et al.* [4] compensated high frequency (25 kHz) dynamometer distortions through a 3×3 force-to-force frequency response function (FRF) inverse filter. Scippa *et al.* [12] designed two Kalman-like filters, "band-fitting" and "parallel elaboration", to compensate for high frequency attenuation of cutting forces.

There are several advantages in using a flexure-based dynamometer. Flexure mechanisms are simple and inexpensive to manufacture and assemble; further, complete mechanisms can be produced from a single monolith. For dynamic measurements, a linear relationship is observed between applied force and displacement for small distortions [13]. The displacement characteristics are smooth and continuous, while providing predictable and repeatable motion. A vibration transducer with high resolution, signal-to-noise ratio, and linearity is therefore able to accurately deconvolve dynamic forces.

In this paper, a method for accurate determination of cutting forces using the FRF is demonstrated for single degree of freedom (SDOF) and multiple degree of freedom (MDOF) flexure-based dynamometers. Structural deconvolution is carried out by applying a filter based on the flexure's inverted FRF to the measured dynamic displacement. This filtered displacement provides the dynamic force.

2. Structural deconvolution

A simulation was coded in MATLAB® to model the deconvolution of the structural dynamics for a SDOF flexure. The first step in performing the deconvolution was to measure the flexure's FRF; see Fig. 1. This was completed by impact testing, where an instrumented hammer is used to excite the structure and a measurement transducer is used to record the resulting vibration [14]. Using the flexure's modal mass, damping, and stiffness, the solution to the differential equation of motion was obtained by numerical integration in the time domain; see Eq. 2, where m is the mass, c is the viscous damping coefficient, k is the stiffness, x is the displacement, the overdots indicate time derivatives, and $F(t)$ is the externally applied force that is to be determined from the displacement signal.

$$m\ddot{x} + c\dot{x} + kx = F(t) \tag{1}$$

Figure 2 shows the externally applied force (top panel) and corresponding displacement (bottom panel) due to this force. The known force was prescribed in Eq. 1 and the corresponding displacement was determined by numerical integration. It is seen that the total solution includes both the transient (homogeneous) and steady-state (particular) solutions.

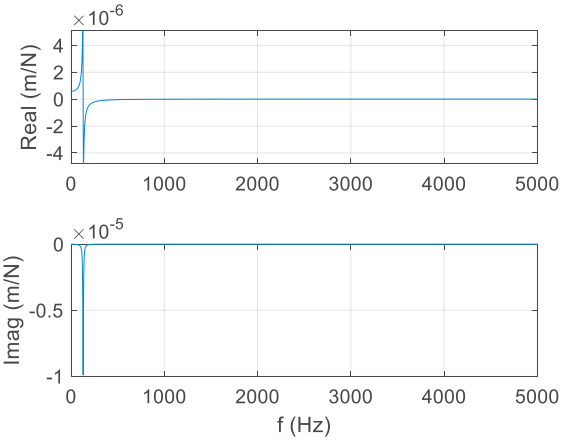

Fig. 1. FRF for the SDOF simulation. (Top) Real part. (Bottom) Imaginary part. The natural frequency is 130 Hz.

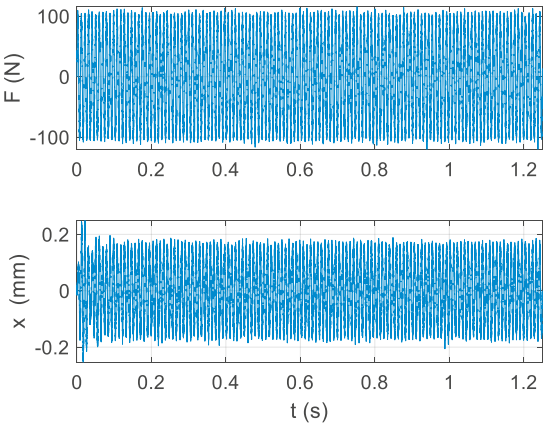

Fig. 2. (Top) Externally applied force. (Bottom) Time domain response of the SDOF system due to the applied force. The displacement was calculated using numerical integration.

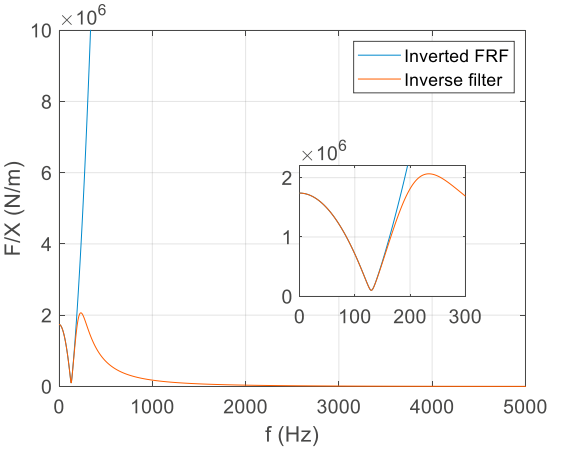

Fig. 3. Inverted flexure FRF and the inverse filter used to remove the influence of the SDOF system dynamics.

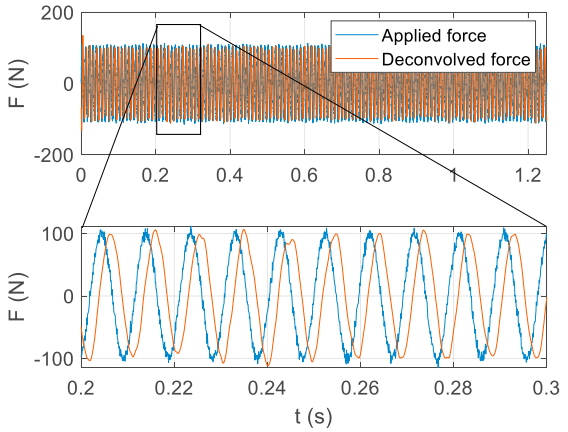

Fig. 4. Comparison of applied and deconvolved forces. A 5% noise level was added to the force and displacement signals.

The structural deconvolution proceeded by: 1) converting the "measured" displacement from Fig. 2 into the frequency domain using the discrete Fourier transform; 2) filtering this signal using the flexure's FRF; and 3) converting the derived force signal back into the time domain using the inverse Fourier transform. The displacement-to-force (receptance) FRF was used to generate a filter which was applied to the frequency-domain displacement to determine the frequency-domain force; this filter is shown in Fig 3. A 4th order lowpass Butterworth filter (200 Hz cutoff frequency) was multiplied by the inverted FRF to remove the effects of the high frequency content amplification due to the FRF inversion. In general, the lowpass filter parameters should consider the dynamics of the flexure system and the forcing frequency. In this instance, 200 Hz was selected as the cutoff frequency.

Figure 4 shows a comparison between the applied and deconvolved force signals. Because noise is always present, a 5% noise level was added to the force and displacement signals. It is observed that the deconvolved force matches well with the known applied force, even in the presence of noise.

To illustrate the ability of this technique to reconstruct cutting forces, a time domain simulation was used to calculate the forces and displacements during milling [1]. The simulation implemented for this study is based on the "regenerative force, dynamic deflection" model described by Smith and Tlusty [15]. The simulation steps are summarized here.

1. The instantaneous chip thickness was determined using the vibration of the previous and current teeth at the selected tooth angle.
2. The cutting force components were calculated as the product of the chip width (axial depth), chip thickness, and specific force coefficients.
3. The force was used to find the new displacement by Euler (numerical) integration of the second order, time delay differential equations of motion.
4. The tooth angle was incremented and the process was repeated.

The simulation was performed for stable, down milling conditions at 4000 rpm. The radial and axial depths of cut were 3 mm and 4 mm, respectively. The commanded feed per tooth was 0.15 µm/tooth for a two-flute cutter. The specific cutting force coefficient that related the resultant force to the chip area was 150 N/mm^2 and the force angle was 60 deg. The simulation and deconvolution results are shown in Figs. 5 and 6. Good agreement between the two force signals is observed.

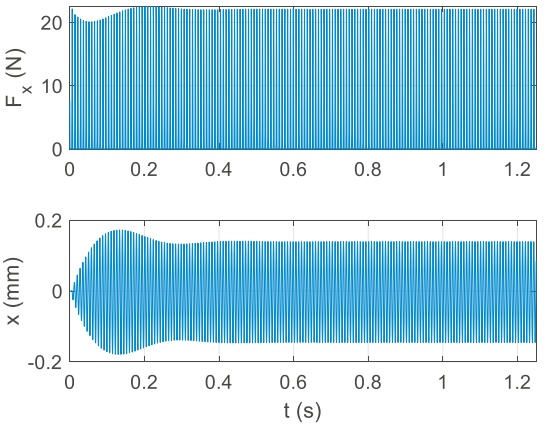

Fig. 5. (Top) Cutting force from time domain simulation. (Bottom) Tool displacement in the feed (x) direction due to the cutting force.

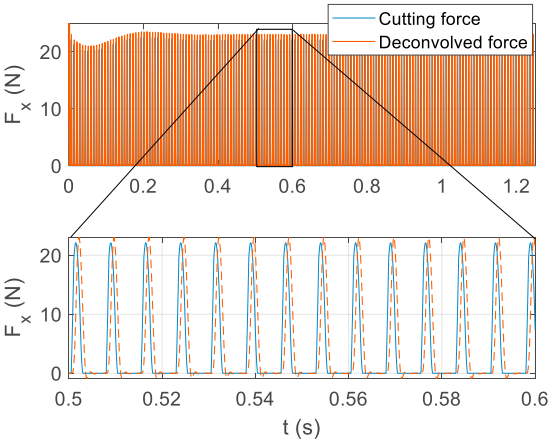

Fig. 6. Comparison of cutting force and deconvolved force.

3. Experimental setup

The experimental setup for the first set of force measurements is illustrated in Fig. 7. A function generator (Tektronix AFG 3022B) was used to command a waveform into a modal shaker (TV 51075-M) which then excited the SDOF flexure through a stinger, which supports axial tension and compression, but not bending or shear [14]. A piezoelectric load cell (PCB 086C04) was attached to one end of the stinger to measure the excitation force applied to the flexure. The corresponding flexure displacement was measured using a capacitance probe (LION Precision C-18-13-2.0).

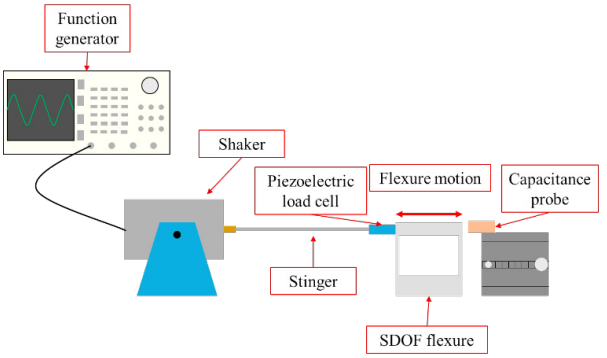

Fig. 7. Experimental setup for SDOF force measurement.

The flexure FRFs were measured by impact testing; the response was measured using a low mass accelerometer (PCB 352C23). The modal parameters for the flexible direction (x) are provided in Table 1.

Table 1. Modal parameters and flexure geometry for the SDOF force measurement setup.

Modal parameters			
Direction	m (kg)	k (N/m)	c (N-s/m)
x	2.456	1.74×10^6	118
Flexure geometry			
Direction	Length (mm)	Width (mm)	Thickness (mm)
x	90	100	5

In a second set of tests, a MDOF flexure stage was used. Details on the design and manufacture of the MDOF flexure stage are provided in [16-17]. The MDOF stage was composed of two parallelogram, leaf-type flexures in an orthogonal, nested orientation; see Fig. 9. Similar to the experimental setup described by Fig. 7, the function generator and modal shaker were used to excite the MDOF system through a stinger. The shaker and stinger were oriented at an angle to excite both directions; see Fig 8. The angle of excitation was determined using the inverse tangent of the resulting y and x direction displacement signals, respectively. The receptance FRF and the resulting inverse filter are shown in Figs. 10-11. The low pass filter had a cutoff frequency of 500 Hz.

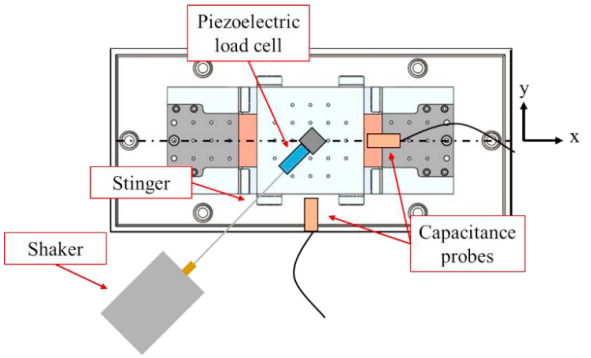

Fig. 8. Experimental setup for MDOF force measurement.

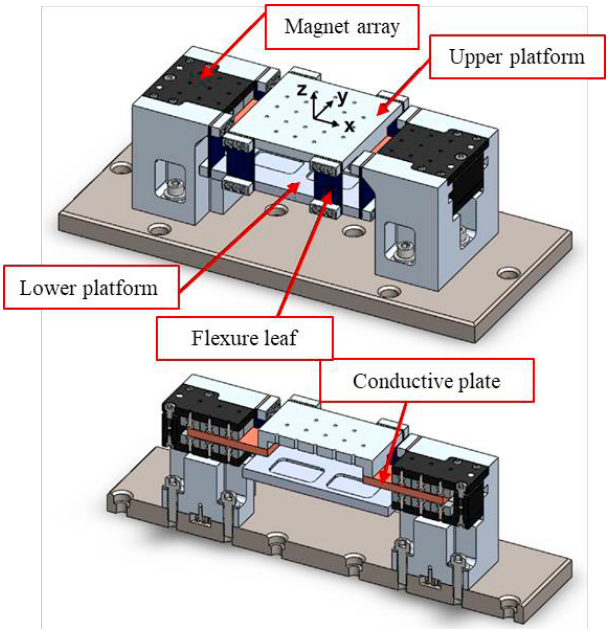

Fig. 9. Assembly view (top) and section view (bottom) for the MDOF flexure. Note that additional damping was provided through eddy current dampers (i.e., a conductive plate moving in a magnetic field).

A series of waveforms were used to demonstrate the ability to reproduce excitation forces from measured displacement and structural deconvolution. The commanded waveforms are summarized in Table 2. Note that the sine and ramp waves contain only the fundamental forcing frequency, while the square and Gaussian waves contain additional content occurring at integer multiples of the forcing frequency.

Table 3. Commanded waveforms produced by the function generator and shaker.

SDOF force measurement	
Waveform	Forcing frequency (Hz)
Sine	5
Ramp	5
Square	20
Gaussian	50
MDOF force measurement	
Waveform	Forcing frequency (Hz)
Sine	50, 100
Square	50, 100
Gaussian	50, 100, 150

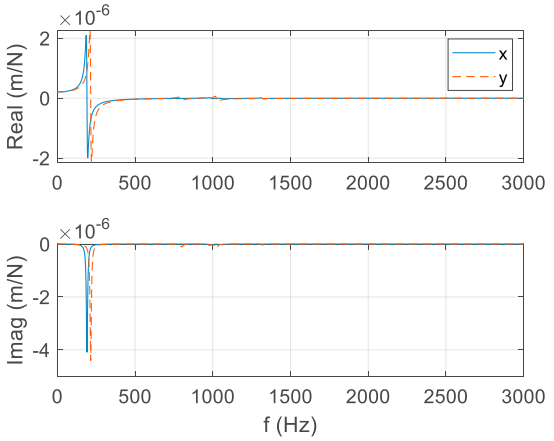

Fig. 10. FRFs for the MDOF flexure force measurement setup. (Top) Real part. (Bottom) Imaginary part.

Table 2. Modal parameters and flexure geometry for the MDOF force measurement.

Modal parameters			
Direction	m (kg)	k (N/m)	c (N-s/m)
x	3.403	4.89×10^{6}	204
x	35.80	1.38×10^{9}	5424
x	27.21	1.20×10^{9}	7987
x	39.45	2.71×10^{9}	3531
y	2.70	4.91×10^{6}	168
y	15.07	3.81×10^{8}	2030
y	34.15	1.29×10^{9}	4032
y	8.55	3.54×10^{8}	902
Flexure geometry			
Direction	Length (mm)	Width (mm)	Thickness (mm)
x	45	35	3.18
y	45	35	3.18

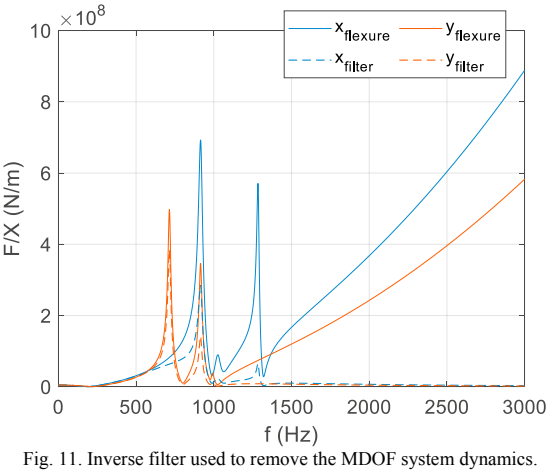

Fig. 11. Inverse filter used to remove the MDOF system dynamics.

Finally, tests were completed where the SDOF flexure was used to determine cutting forces in a set of milling tests. First, a set of cutting tests were carried out by mounting an aluminum workpiece on a multi-axis piezoelectric dynamometer (Kistler 9257B). The second set of cutting tests were performed by mounting the workpiece on the SDOF flexure, where the flexure displacement was measured using a capacitance probe; see Fig. 12.

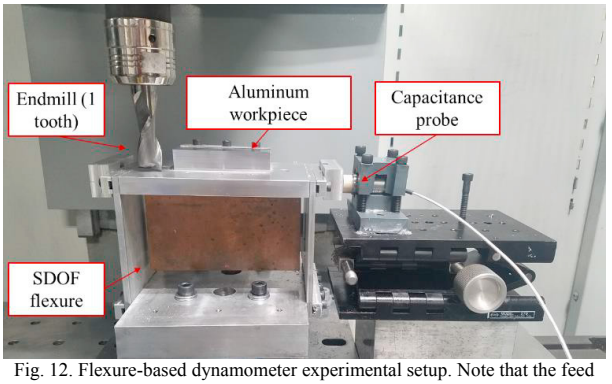

Fig. 12. Flexure-based dynamometer experimental setup. Note that the feed direction is in the flexible direction for the flexure.

Stable down milling conditions were selected for all trials with a spindle speed of 2550 rpm. The radial and axial depths of cut were both 2 mm. A set of five feed rates were selected: {25, 50, 75, 100, and 125} μm/tooth.

Table 4. Modal parameters and flexure geometry for the SDOF cutting force measurement.

Modal parameters			
Direction	m (kg)	k (N/m)	c (N-s/m)
x	2.75	1.74×10^{6}	39
Flexure geometry			
Direction	Length (mm)	Width (mm)	Thickness (mm)
x	90	100	5

4. Results

Measured and deconvolved forces for the SDOF shaker flexure experiment are shown in Figs. 13-17. Good agreement is observed in all cases with minor discrepancies in amplitude. The differences can be attributed to the low pass filter which attenuates higher-order frequencies which may be present in the forcing function. The low pass cutoff frequency was set at 10 times the forcing frequency in each case.

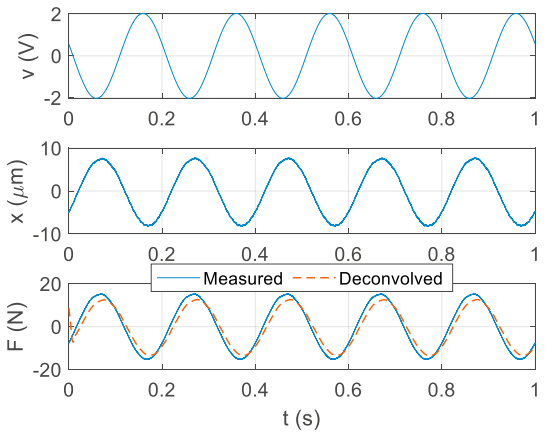

Fig. 13. Time domain signals for a 5 Hz sine wave. (Top) Commanded voltage from function generator. (Middle) Measured displacement. (Bottom) Force signals.

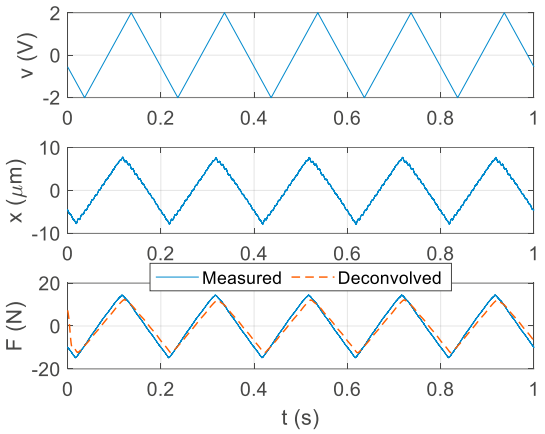

Fig. 14. Time domain signals for 5 Hz ramp wave.

Frequently, partial radial immersion cutting forces resemble trains of periodic impulses [1]. Therefore, the Gaussian waves were used to simulate the forces that may be encountered during milling operations; see Figs. 16 and 17.

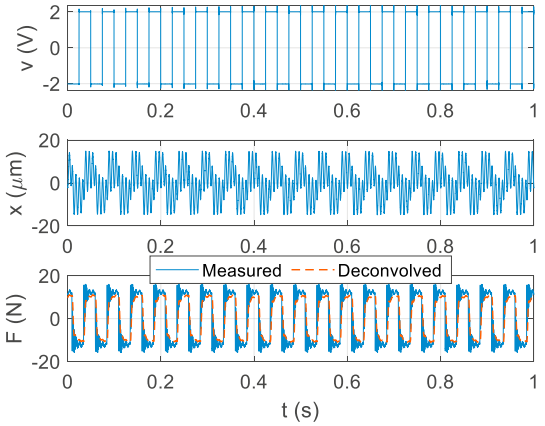

Fig. 15. Time domain signals for 20 Hz square wave.

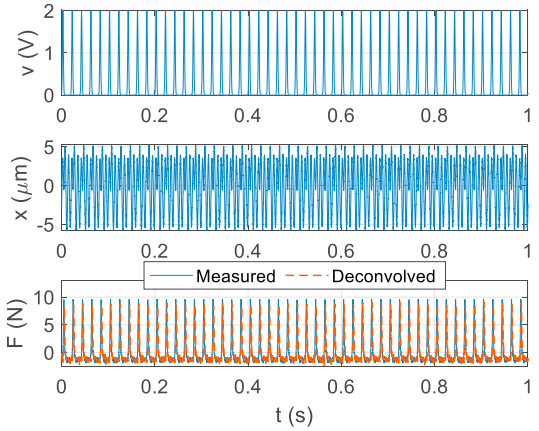

Fig. 16. Time domain signals for 50 Hz Gaussian wave.

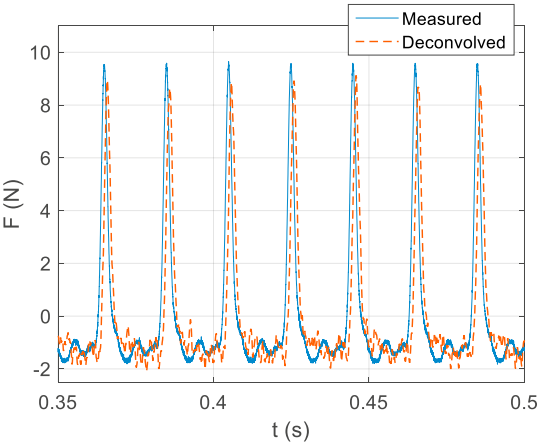

Fig. 17. Time domain force signals for 50 Hz Gaussian wave.

Results for the MDOF setup (Fig. 9) are presented in Figs. 18-24 for multiple waveforms and forcing frequencies. For brevity, only for force results are shown. However, the deconvolved forces were again determined from the measured displacements and MODF structural dynamics. Good agreement is generally observed. For the low pass filter, a cutoff frequency of 500 Hz was selected.

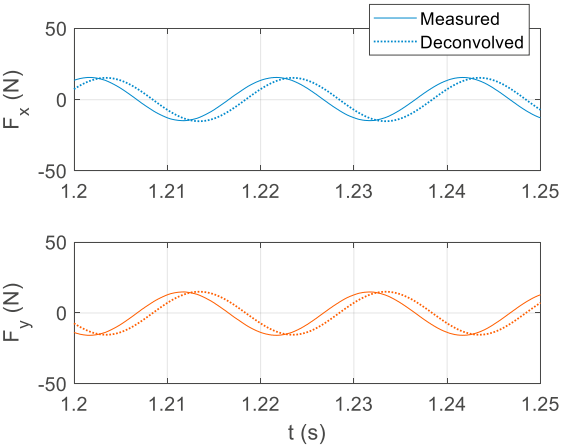

Fig. 18. Time domain force signals for 50 Hz sine wave.

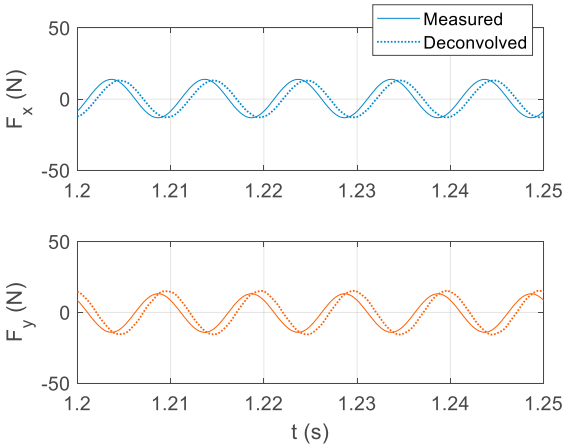

Fig. 19. Time domain force signals for a 100 Hz sine wave.

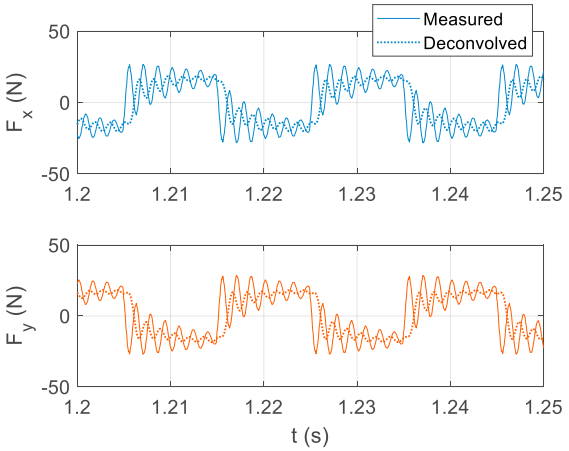

Fig. 20. Time domain force signals for a 50 Hz square wave.

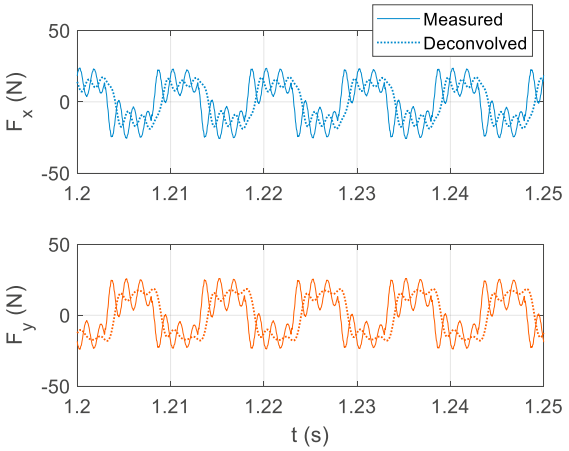

Fig. 21. Time domain force signals for a 100 Hz square wave.

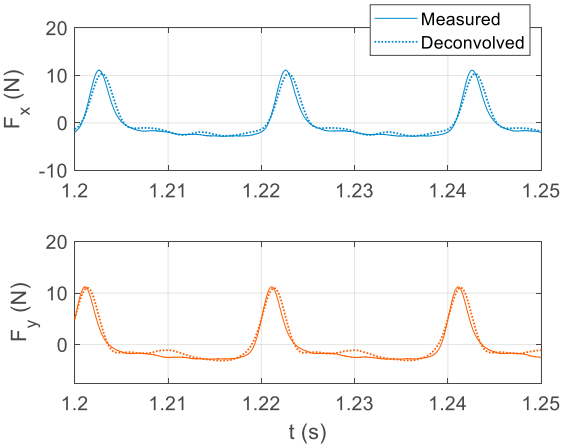

Fig. 22. Time domain force signals for a 50 Hz Gaussian wave.

At higher forcing frequencies, the deconvolved results are affected by the low pass cutoff. With higher cutoff frequencies the noise increases, so a balance is required. To increase the cutoff frequency, a flexure-based dynamometer with a higher natural frequency can be designed and constructed.

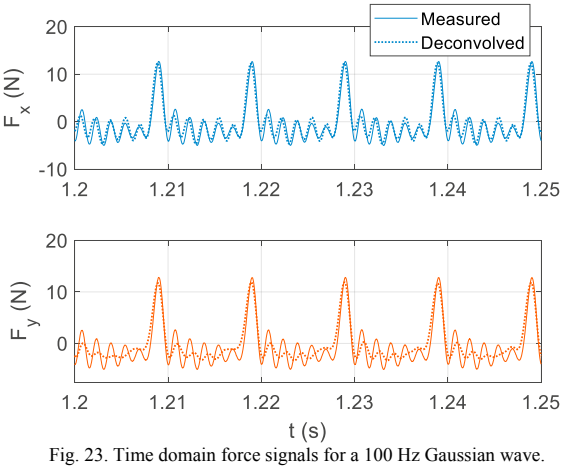

Fig. 23. Time domain force signals for a 100 Hz Gaussian wave.

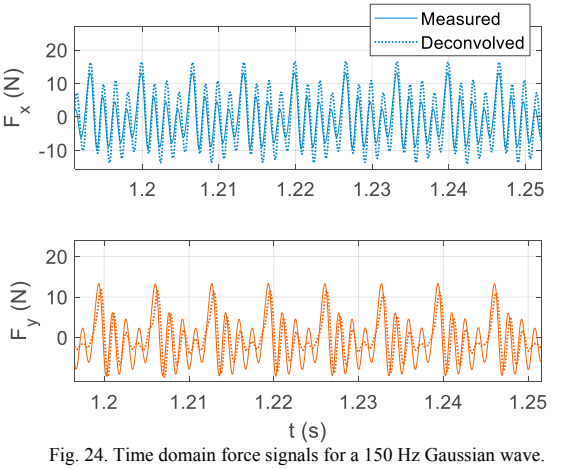

Fig. 24. Time domain force signals for a 150 Hz Gaussian wave.

Finally, a comparison of milling force signals is provided for the SDOF setup (Fig. 12). The flexure's displacement was

used to calculate the applied cutting force. The low pass filter for the deconvolution step had a cutoff frequency of 425 Hz. Additionally, a separate low pass filter was applied to the cutting forces measured by the piezoelectric-based dynamometer to attenuate the high frequency content introduced by the dynamometer dynamics (1500 Hz cutoff frequency). The results are displayed in Figs. 25-29. Good agreement is observed.

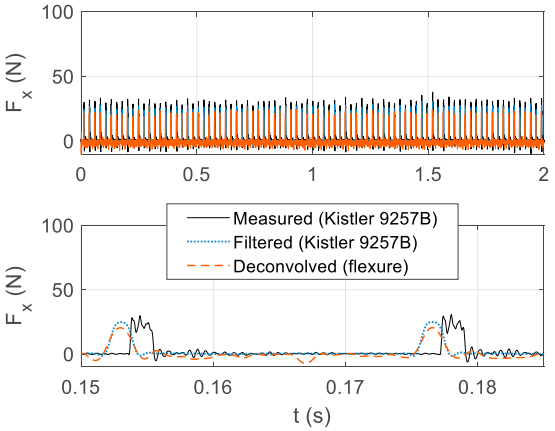

Fig. 25. Measured, filtered, and calculated cutting forces (25µm/tooth).

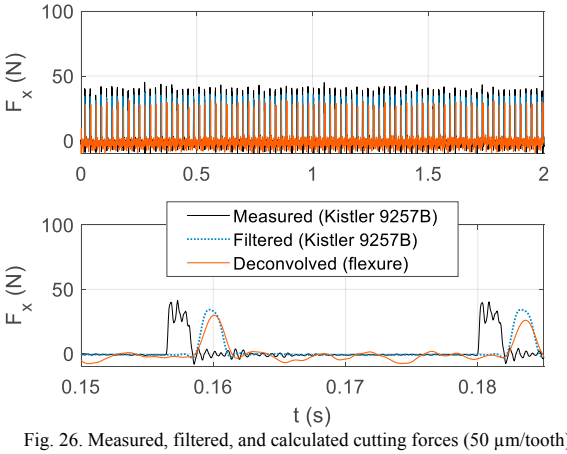

Fig. 26. Measured, filtered, and calculated cutting forces (50 µm/tooth).

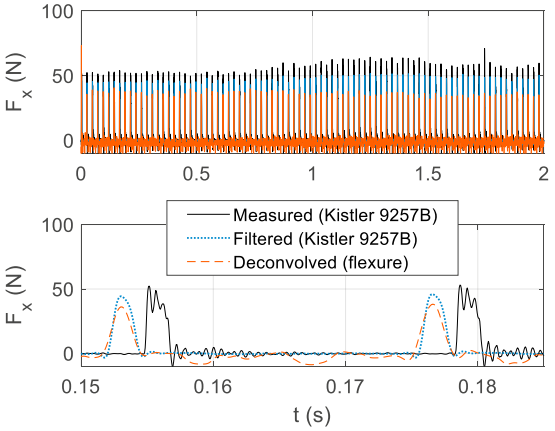

Fig. 27. Measured, filtered, and calculated cutting forces (75 µm/tooth).

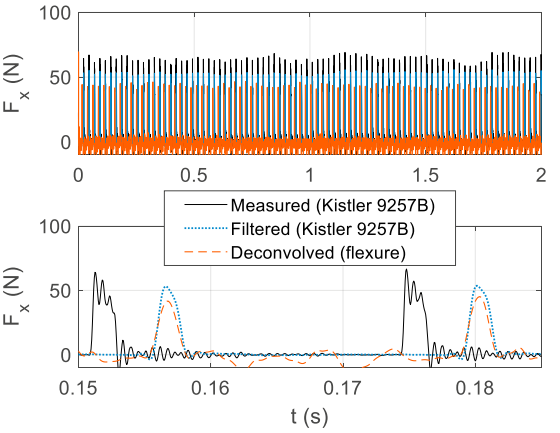

Fig. 28. Measured, filtered, and calculated cutting forces (100 µm/tooth).

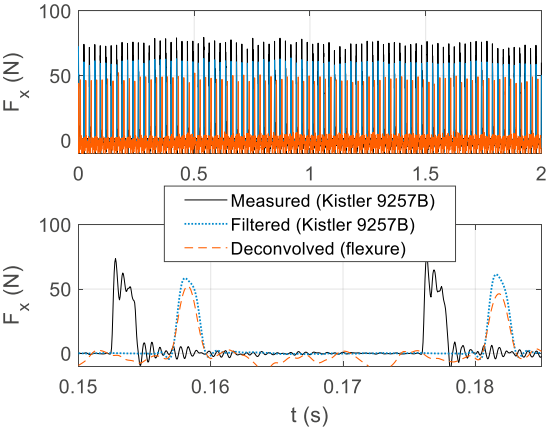

Fig. 29. Measured, filtered, and calculated cutting forces (125 µm/tooth).

Discrepancies in force amplitude are caused by additional frequency content introduced by the dynamometer's structural dynamics. The artificial amplification leads to appreciable error in cutting force measurement. The frequency content for the 125 µm/tooth case is displayed in Fig. 30.

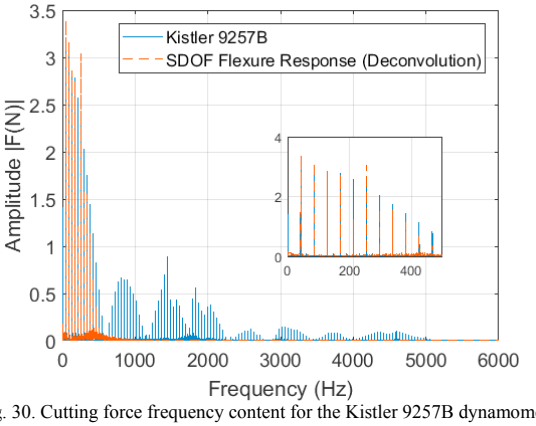

Fig. 30. Cutting force frequency content for the Kistler 9257B dynamometer and the SDOF flexure-based dynamometer.

5. Conclusions

The purpose of this paper was to demonstrate the ability to measure cutting forces using a displacement-based approach. The physical implementation included a flexure-based strategy where structural deconvolution was carried out by filtering the measured displacement signals using the flexure's inverted receptance FRF. A low pass filter was also applied to attenuate the high frequency noise amplification caused by the flexure FRF inversion. It was shown that, for a variety of excitation forces, the measured displacement could be used to reconstruct the force profile for both SDOF and MDOF flexure-based dynamometers.

It was found that it is important to consider the signal-to-noise ratio for the displacement transducer because the frequency domain filtering step is sensitive to noise. In continuing this research, low-cost, low-noise optical displacement sensors will be used to measure the flexure vibration. Additionally, an uncertainty analysis will be developed for the cutting force signal. In doing so, accurate, low-cost force measurement will be enabled. New flexure designs with higher natural frequencies will be applied to increase measurement bandwidth during machining processes.

Acknowledgements

The authors gratefully acknowledge partial financial support from the UNC Charlotte Center for Precision Metrology.

References

[1] Schmitz, T.L., Smith, K.S., 2009, Machining Dynamics: Frequency Response to Improved Productivity, Springer, New York, NY.

[2] Altintas, Y., 2012, Manufacturing Automation: Metal Cutting Mechanics, Machine Tool Vibrations, and CNC Design, Cambridge University Press.

[3] Castro, L.R., Vieville, P., Lipinski, P., 2006, Correction of dynamic effects on force mesurements made with piezoelectric dynamometers, International Journal of Machine Tools & Manufacture, 46, 1707-1715.

[4] Ozdoganlar, O.B., Korkmaz, E., Gozen, B.A., Bediz, B., 2015, High-frequency compensation of dynamic distortions in micromachining force measurments, Procedia Manufacturing, 1, 534-545.

[5] Rubeo, M.A., and Schmitz, T.L., 2016, Mechanistic force model coefficients: A comparison of linear regression and nonlinear optimization, Precision Engineering, 45, 311-321.

[6] Burton, D., Duncan, G.S., Ziegert, J.C., Schmitz, T.L., 2004, High frequency, low force dynamometer for micro-milling force measurement, Proceedings of the 19th American Society for Precision Eningeering Anuual Meeting, 221-224.

[7] Yaldiz, S., Unsacar, F., Haci, S., Isik, H., 2007, Design, development and testing of a four-component milling dynamometer for the measurement of cutting force and torque, Mechanical Systems and Signal Processing, 21, 1499-1511.

[8] Transchel, R. Stirnimann, J., Blattner, M., Bill, B., Thiel,R., Kuster, F., Wegener, K, 2012, Effective dynamometer for measuring high dynamic process force signals in micro machining operations, Procedia CIRP, 1, 558-562.

[9] Totis, G., Adams, O., Sortino, M., Veselovac, D. Klocke, F., 2014, Development of an innovative plate dynamometer for advanced milling and drilling applications, Measurement, 49, 164-181.

[10] Ettrichratz, M., Drossel, W., Gebhardt, S., Bucht, A., Kranz, B., Schneider, J., 2018, Performance of a new piezoceramic thick film sensor for measurement and control of cutting forces during milling, CIRP Annals, 67/1, 45-48.

[11] Altintas Y., and Park S.S., 2004, Dynamic compensation of spindle-integrated force sensors, CIRP Annals, 53/1, 305-308.

[12] Scippa, A., Sallese, L., Grossi, N., Campatelli, G., 2015, Improved dynamic compensation for accurate cutting force measurements in milling applications, Mechanical Systems and Signal Processing, 54-55, 314-324.

[13] Smith, S.T., 2000, Flexures: Elements of Elastic Mechanisms, CRC Press, Boca Raton, FL.

[14] Schmitz, T.L., Smith, K.S., 2012, Mechanical Vibrations: Modeling and Measurement, Springer, New York, NY.

[15] Smith, K.S., and Tlusty, J., 1991, An overview of modeling and simulation of the milling process, ASME Journal of Engineering for Industry, 113/2, 169-175.

[16] Rubeo, M.A., Kiran, K., Schmitz, T.L., 2016, The design of a multiple degree of freedom flexure stage with tunable dynamics for milling experimentation, Transactions of the NAMRI/SME, 44.

[17] Kiran, K., Rubeo, M.A., Kayacan, C., and Schmitz T.L., 2017, Two degree of freedom frequency domain surface location error predition, Precision Engineering, 48, 234-242.